Neutron Diffraction Study of $Ba_6Mn_4MO_{15}$ (M = Cu, Zn): Long-Range Magnetic Order in Pseudo-1D Materials

Edmund J. Cussen, Jaap F. Vente,† and Peter D. Battle*

Contribution from the Inorganic Chemistry Laboratory, University of Oxford, South Parks Road, Oxford OX1 3QR, U.K.

Received December 14, 1998

Abstract: The room-temperature crystal structures of $Ba_6Mn_4MO_{15}$ (M = Zn, Cu) have been refined using X-ray and neutron powder diffraction data simultaneously. $Ba_6Mn_4ZnO_{15}$ is isostructural with $Ba_6Ni_5O_{15}$ and contains transition metals in chains of oxide polyhedra (trigonal prisms and octahedra); neighboring chains are separated from each other by the Ba atoms. Zn and Mn occupy the trigonal prismatic site in equal concentrations, with the remaining Zn and Mn partially ordered over the two crystallographically distinct octahedral sites. The neutron diffraction data show $Ba_6Mn_4CuO_{15}$ to adopt a very similar structure but reveal that Cu is displaced from the center of the trigonal prism to give pseudo-square-planar coordination. A neutron diffraction experiment performed at 1.7 K showed additional intensity due to long-range magnetic order on the octahedral sites, and this has been modeled using an unusual magnetic structure in which the antiferromagnetic superexchange within the highly frustrated crystal structure leads to a rotation of 120° between spins in neighboring chains. The magnetic moments refined to 0.16(2) and 0.12(3) μ_B per octahedral site in the Cu and Zn compounds, respectively. The magnetic susceptibility of $Ba_6Mn_4CuO_{15}$ is consistent with the trigonal prismatic Cu remaining paramagnetic in the range $5 \leq T/K \leq 300$, in which case the contribution to the susceptibility from the octahedrally coordinated Mn is qualitatively similar to the observed susceptibility of $Ba_6Mn_4ZnO_{15}$, showing a broad maximum (90(5) K for M = Cu, 45(5) K for M = Zn) indicative of 1-dimensional ordering. In neither compound is it possible to identify the Néel temperature, although the susceptibility of $Ba_6Mn_4CuO_{15}$ suggests that the Cu spins in trigonal prismatic coordination freeze at 5 K, and it is likely that this coincides with the onset of long-range magnetic ordering on the octahedral sites.

Introduction

Recently, there has been a growth in interest[1−3] in a group of materials structurally related to Sr_4PtO_6.[4] In that compound, SrO_6 and PtO_6 polyhedra (trigonal prisms and octahedra, respectively) share triangular faces to form 1:1 chains parallel to the *z* axis of a rhombohedral unit cell; the chains are separated by the remaining Sr cations. The current research activity was born of the realization that this structure is related to the 2H perovskite compounds, for example, $BaNiO_3$,[5] which contains chains of face-sharing octahedra parallel to *z*. The 2H perovskite ABO_3 can also be considered to contain hexagonal close-packed layers of stoichiometry A_3O_9, with the B cations occupying the resulting face-sharing, 6-coordinate interstitial sites. The Sr_4PtO_6 structure type can be derived from this by removing one-third of the oxygen atoms from each layer to give the stoichiometry A_3O_6, thus creating a void that can accommodate a cation, A′, in trigonal prismatic coordination and, hence, a layer of stoichiometry $A_3A'O_6$. This trigonal prismatic site within the layer has nominally replaced two interlayer octahedral sites and so it is the larger of the two types of 6-coordinate site, although in practice the size difference is reduced by buckling of the layers. The Sr_4PtO_6 structure (A = A′ = Sr) results if every layer in the structure has stoichiometry $A_3A'O_6$. However, if layers of composition A_3O_9 are inserted into the stacking sequence, it is possible to generate a large number of structures that contain different numbers of octahedra separating the trigonal prismatic sites in the chain. Darriet and Subramanian[6] have described a labeling scheme in which the structure can be described by the number, *n*, of consecutive $A_3A'O_6$ layers on either side of a single A_3O_9 layer. In this description the Sr_4PtO_6 structure corresponds to $n = \infty$, while the perovskite is the $n = 0$ end member. Much of the published work on these materials has been on Ni- or Co-containing compounds,[7,8] presumably as a result of $BaNiO_3$[5] and $BaCoO_{3-\delta}$[9] both being known to adopt the 2H structure. However, materials based on the only other reported 2H oxide, $BaMnO_3$, have received little attention. We present here the first full structural study of Mn-containing mixed-layer compounds, the $n = 1$ phases $Ba_6Mn_4ZnO_{15}$ and $Ba_6Mn_4CuO_{15}$, and the first magnetic structure determination of a mixed layer compound having $n \neq \infty$. The idealized, rhombohedral structure of these phases is drawn in Figure 1, which shows chains of oxide polyhedra separated by

* To whom correspondence should be addressed.
†Present address: Cinvestav-IPN Unidad Merida, Departemento de Fisica Aplicada, Carretera Ant. a Progreso km 6, Apartado Postal #73 Cordemex, Merida, Yucatan 97310, Mexico.

(1) Blake, G. R.; Sloan, J.; Vente, J. F.; Battle, P. D. *Chem. Mater.* **1998**, *10*, 3536.
(2) Nguyen, T. N.; zur-Loye, H. C. *J. Solid State Chem.* **1995**, *117*, 300.
(3) Dussarrat, C.; Fompeyrine, J.; Darriet, J. *Eur. J. Solid State Chem.* **1995**, *32*, 3.
(4) Randall, J. J.; Katz, L. *Acta Crystallogr.* **1959**, *12*, 519.
(5) Lander, J. J. *Acta Crstallogr.* **1951**, *4*, 148.
(6) Darriet, J.; Subramanian, M. A. *J. Mater. Chem.* **1995**, *5*, 543.
(7) Campa, J. A.; Guitierrez-Puebla, E.; Monge, M. A.; Rasines, I.; Ruiz-Valero, C. *J. Solid State Chem.* **1994**, *108*, 230.
(8) Harrison, W. T. A.; Hegwood, S. L.; Jacobson, A. J. *Chem. Commun.* **1995**, 1952.
(9) Taguchi, H.; Shimada, M.; Kanamaru, F.; Koizumi, M.; Takeda, Y. *J. Solid State Chem.* **1976**, *18*, 299.

10.1021/ja984313u CCC: $18.00
Published on Web 04/13/1999

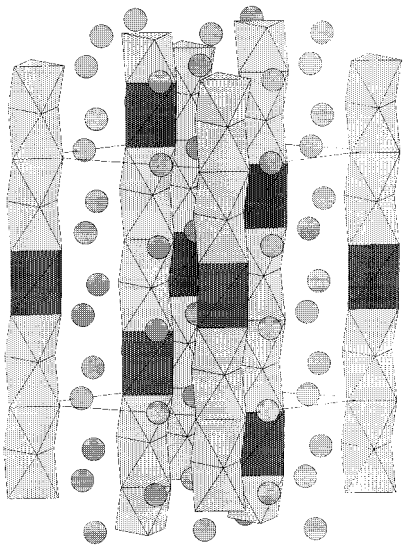

Figure 1. Ideal crystal structure of $Ba_6Mn_4MO_{15}$: circles represent Ba cations, transition metal coordination is shown by shaded trigonal prisms (dark) and octahedra (light).

Ba cations. The transition metals are accommodated in these chains, which contain tetramers of octahedral sites separated by a single prismatic site; the rhombohedral symmetry ensures that the trigonal prisms are found in different layers in each of the chains.

Experimental Section

Samples of $Ba_6Mn_4ZnO_{15}$ and $Ba_6Mn_4CuO_{15}$ were prepared using standard solid-state techniques. Stoichiometric mixtures of $BaCO_3$, MnO_2, and ZnO/CuO were thoroughly ground using an agate mortar and pestle and decarbonated at 800 °C for 1 day before being pelleted and heated at 1000 °C for 2 days and 1050 °C for 8 days. The two compounds then underwent different heat treatments. The Cu-containing sample was heated at 1090 °C for 2.5 h, 1120 °C for 1.5 h, and 1125 °C for 2 h. The Zn-containing compound was heated at 1090 °C for 24 h, 1130 °C for 18 h, 1140 °C for 24 h, 1170 °C for 6 h, and 1200 °C for 9.5 h. The progress of the reactions was followed by X-ray powder diffraction. During the earlier stages of the preparation the X-ray diffraction data collected from the samples contained no extra peaks indicative of second-phase contaminants, but the patterns could not be indexed using a single set of lattice parameters in the usual manner of a commensurate compound. Instead, the pattern could only be satisfactorily indexed using two *c* parameters in a manner we have described previously in our discussion of related incommensurate structures.[1] The first parameter, c_1, corresponds to the *aba* repeat distance in the BaO_3 stack familiar from the 2H perovskite structure, while the second parameter, c_2, is the average metal−metal distance in the chain of transition-metal polyhedra. For an $n = 1$ structure, with a total of six layers per unit cell, $c_1/c_2 = 5/3$,[1] and this ratio yields a straightforward method of describing the magnitude of the incommensuration. The XRD patterns collected in the early stages of synthesis could be indexed with $c_1/c_2 < 5/3$. Further heating increased the value of c_1/c_2 until the samples were judged to be commensurate with $c_1/c_2 = 5/3$ within experimental error, hence permitting the use of a single c parameter ($c = 3c_1 = 5c_2$). Overheating resulted in $c_1/c_2 > 5/3$, and the preparation had to be recommenced. X-ray diffraction data were collected from the final products in the angular range $10 \leq 2\theta/° \leq 120$ in steps of $\Delta 2\theta = 0.02°$ using a Siemens D5000 diffractometer operating with Cu−Kα_1 radiation in Bragg−Brentano geometry. Neutron diffraction data were collected in the angular range $10 \leq 2\theta/° \leq 148$ in steps of $\Delta 2\theta = 0.05°$, $\lambda = 1.5938$ Å, on the diffractometer D2b at the Institut Laue-Langevin in Grenoble at both 290 and 1.70 K. The sample, ca. 5.5 g, was contained in a 16 mm diameter vanadium can and the temperature was controlled by an orange ILL cryostat giving a temperature stability of ±0.08 K at 1.70 K.

All the diffraction data, uncorrected for absorption, were analyzed by profile analysis[10] using the GSAS suite of programs.[11] The background was fitted by a Chebyshev polynomial, and the peak shape was described by a pseudo-Voigt function. Magnetic measurements were performed using a Quantum Design SQUID magnetometer. The susceptibilities were recorded in fields of 100 and 1000 G after cooling in both zero field (ZFC) and the measuring field (FC), and measurements of magnetization as a function of field were carried out between +10 kG and −10 kG after cooling in a field of +10 kG.

Results

The preparation of these materials as commensurate phases is challenging and requires extremely accurate control of both temperature and heating time: a difference of 10 °C can change the degree of commensuration greatly, and heating times of less than 1 h can cause the compound to pass from under commensurate to over commensurate. We do not, as yet, fully understand the cause of this behavior. A consequent problem is that heat treatments must be stopped when the material is commensurate—it is not possible to heat the material further to increase the crystallinity of the sample. The commensurate nature of our samples was verified by accurately determining the individual peak positions in the neutron data using a Gaussian function to describe the peak shape. The peaks were indexed using the c_1, c_2 formalism, and the four lattice parameters were determined by a least-squares refinement. The resulting lattice parameters based on the room-temperature neutron diffraction data gave values of c_1/c_2 of 1.6666(2) and 1.666(2) for $Ba_6Mn_4CuO_{15}$ and $Ba_6Mn_4ZnO_{15}$, respectively. While both values are in excellent agreement with the commensurate value, 5/3, the larger standard deviation in the value from the Zn compound indicates the sample to be of slightly poorer quality; this is a consequence of having to halt the heat treatment when the sample is commensurate rather when instrumental peak widths are obtained in the diffraction pattern.

The distribution of transition metals over the two crystallographically distinct octahedral sites and the trigonal prismatic site in these compounds could not be determined from X-ray diffraction experiments because of the similar scattering factors of Mn and Zn/Cu. Furthermore, due to the dominating influence of the strongly scattering Ba atoms, the X-ray data alone did not contain sufficient information to allow refinements of the transition-metal positions in the trigonal prismatic sites. Rietveld analyses were therefore carried out using simultaneous refinements of the X-ray and neutron diffraction data collected at room temperature. It should be noted that both the X-ray and neutron diffraction patterns showed anisotropic broadening of $l \neq 0$ reflections relative to *hk*0 reflections. This broadening is ascribed to stacking faults in the *c*-direction and is a common observation in these structures.[12]

Initial refinements of the data collected from $Ba_6Mn_4CuO_{15}$ assumed the compound to have the structure drawn in Figure 1, with a fully ordered arrangement of the transition metals over the octahedral and trigonal prismatic sites, the former being occupied by Mn and the latter by Cu. This model gave a poor fit to the neutron diffraction data. The fit was improved considerably by allowing the transition-metal distribution over the three sites to vary with the constraints that the above stoichiometry be maintained and that the isotropic temperature factor be the same at each transition-metal site. Isotropic

(10) Rietveld, H. M. *J. Appl. Crystallogr.* **1969**, *2*, 65.
(11) Larson, A. C.; von Dreele, R. B. *General Structure Analysis System (GSAS)*; Los Alamos National Laboratories: Los Alamos, NM, 1990.
(12) Battle, P. D.; Burley, J. C.; Cussen, E. J.; Darriet, J.; Weill, F. *J. Mater. Chem.* **1999**, *9*, 479.

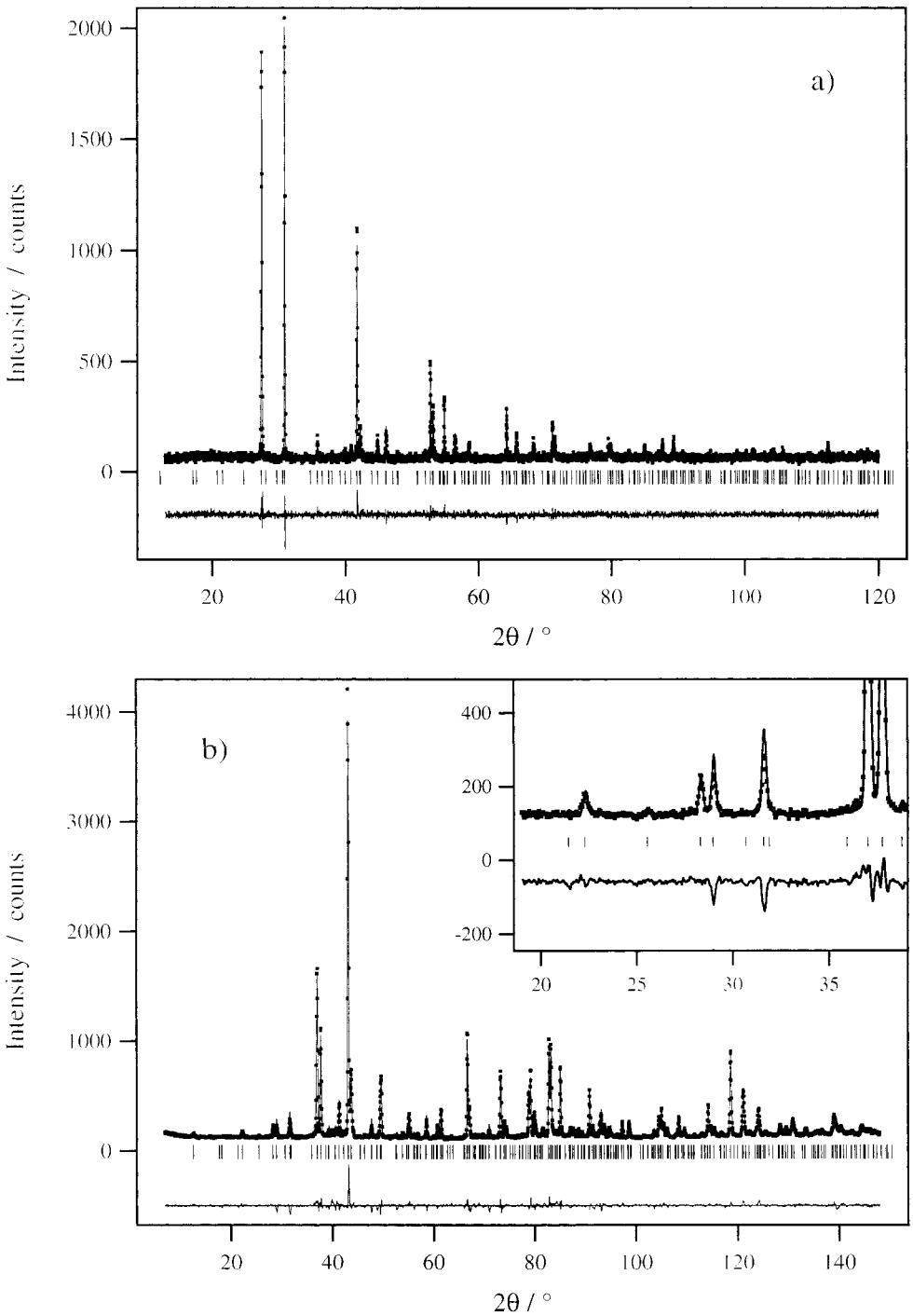

Figure 2. Observed (dots), calculated (full line), and difference X-ray (a) and neutron (b) diffraction patterns from $Ba_6Mn_4CuO_{15}$ at room temperature. The inset in part b shows the absence of magnetic peaks at room temperature. Reflection positions are indicated by tick marks.

temperature factors were refined independently for all other atoms. Although the quality of fit improved, the temperature factor of the transition metals refined to unrealistically large values, indicating our model was still inadequate and a difference Fourier map was therefore calculated. This showed good agreement between the calculated and observed nuclear scattering density on the octahedral sites but showed a deficiency in our model of the trigonal prismatic site; there was considerable positive density toward the rectangular faces of the prism and negative density at the prism center and toward the triangular faces. We modeled the positive difference by displacing the Cu atom from the 3-fold axis at the center of the prism toward the rectangular faces, giving a pseudo-square-planar coordination. The negative difference was due to the unmodeled displacement of Mn ($b = -0.373 \times 10^{-14}$ m), and a substantial improvement in the fit resulted from displacing Mn from the center of the prism toward the triangular faces. The oxygen site occupancies refined to unity and were subsequently fixed at this value. The final refined transition-metal occupancies show the central pair of octahedral sites, M(2), are occupied exclusively by manganese while partial ordering occurs over the other octahedral site M(3), 0.840(5)Mn/0.160(5)Cu, and the trigonal prismatic site, M(1), 0.320(5)Mn/0.680(5)Cu. The final stages of the refinement utilized a total of 60 variables: 2 scale factors, 2 zero points, 1 wavelength, 7 X-ray background, 15 neutron background, 5 X-ray profile, 6 neutron profile, 2 lattice

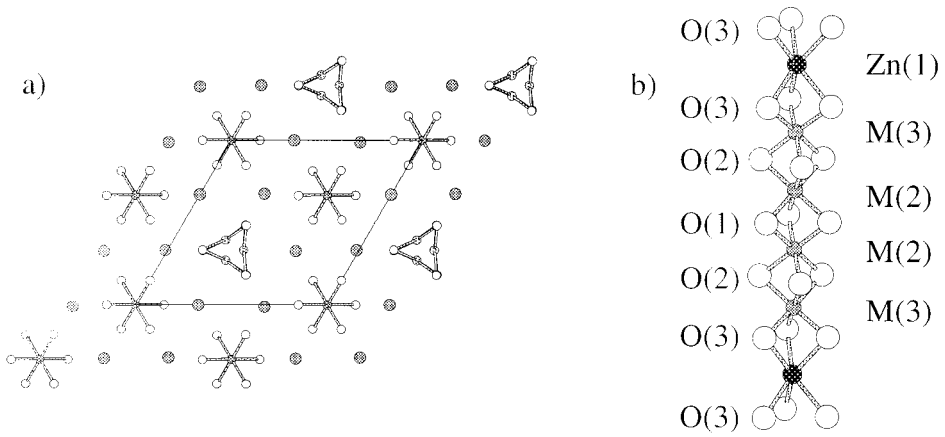

Figure 3. Transition-metal environments showing (a) the [001] projection of a section of $Ba_6Mn_4CuO_{15}$ and (b) a [110] projection of a section of polyhedral chain from $Ba_6Mn_4ZnO_{15}$. Lines show the coordination between oxide ions (white circles) and transition metals. The differences in coordination between Cu and Zn are clear. Mn has been omitted from the trigonal prismatic site in both diagrams for increased clarity.

Table 1. Structural Parameters for $Ba_6Mn_4CuO_{15}$ at Room Temperature[a]

	site	*x*	*y*	*z*	U_{iso}	frac
Ba(1)	9d	0.3275(4)	0	0	0.016(2)	
Ba(2)	9e	0.6550(4)	0	$^1/_2$	0.009(1)	
Cu(1)[b]	9d	0.938(1)	0.938(1)	$^1/_2$	0.0043(8)	0.223(4)
Mn(1)[b]	6c	0	0	0.530(3)	0.0043(8)	0.166(5)
M(2)	6c	0	0	0.0949(7)	0.0043(8)	1
M(3)	6c	0	0	0.289(1)	0.0043(8)	0.834(5) Mn/0.166(5)Cu
O(1)	9d	0.8499(4)	0	0	0.0017(9)	
O(2)	18f	0.4818(5)	−0.3335(5)	0.4798(3)	0.0156(8)	
O(3)	18f	0.8509(4)	0.0020(5)	0.6301(2)	0.0208(6)	

[a] Space group *R*32: $a = 10.0469(3)$ Å, $c = 12.8470(4)$ Å, V = 1123.05(7) Å^3. [b] Disordered from center of trigonal prism. Trigonal prism has fractional occupancy 0.669(4)Cu/0.332(5) Mn.

Table 2. Bond Distances (Å) and Angles (deg) in $Ba_6Mn_4CuO_{15}$ at Room Temperature

Ba(1)−O(1)	2.853(4) × 2	Cu(1)−O(3)	2.130(3) × 2
Ba(1)−O(2)	2.664(4) × 2	Cu(1)−O(3)	2.121(3) × 2
Ba(1)−O(2)	3.000(5) × 2	Cu(1)−O(3)	2.701(8) × 2
Ba(1)−O(3)	2.974(6) × 2	Mn(1)−O(3)	1.98(3) × 3
Ba(1)−O(3)	2.964(4) × 2	Mn(1)−O(3)	2.55(3) × 3
Ba(2)−O(1)	2.788(3) × 2	M(2)−O(1)	1.939(7) × 3
Ba(2)−O(2)	2.914(5) × 2	M(2)−O(2)	1.904(7) × 3
Ba(2)−O(2)	2.820(6) × 2	M(3)−O(2)	1.99(1) × 3
Ba(2)−O(3)	2.574(4) × 2	M(3)−O(3)	1.832(9) × 3
Ba(2)−O(3)	3.164(3) × 2	M(2)−M(3)	2.49(2)
shortest O(2)−O(2)	2.586(7)	M(2)−M(2)	2.44(2)
		Mn(1)−M(3)	2.33(5)
		Cu(1)−M(3)	2.78(1)
O(3)−Cu(1)−O(3)	75.8(2)	O(3)−Mn(1)−O(3)	82(1)
O(3)−Cu(1)−O(3)	64.2(2)	O(3)−Mn(1)−O(3)	94.2(4)
O(3)−Cu(1)−O(3)	173.2(6)	O(2)−M(3)−O(2)	81.2(5)
O(3)−Cu(1)−O(3)	121.9(4)	O(2)−M(3)−O(3)	93.4(2)
O(3)−Cu(1)−O(3)	103.7(2)	O(2)−M(3)−O(3)	94.1(2)
Cu(1)−O(3)−M(3)	72.8(4)	O(1)−M(2)−O(2)	94.9(1)
M(2)−O(2)−M(3)	79.7(4)		

parameters, 6 U_{iso}'s, 1 occupancy, and 13 atomic parameters. The final fit has the residuals $R_{wp} = 12.20$, $R_p = 9.55$, $R_I = 15.31$, DW-d = 1.828 for the X-ray data, shown in Figure 2a, and $R_{wp} = 6.56$, $R_p = 4.93$, $R_I = 5.88$, DW-d = 0.556 for the neutron data, shown in Figure 2b, giving a total $\chi^2_{red} = 2.014$ for the combined refinement. The resulting atomic positions are given in Table 1, and the most important bond distances and angles are presented in Table 2. A section of the structure is shown along the [001] projection in Figure 3a, clearly showing Cu in square-planar coordination.

The room-temperature $Ba_6Mn_4ZnO_{15}$ neutron and X-ray data were refined simultaneously in a manner similar to that described above. Substantial structural differences between the compounds are only evident in the transition-metal chains, the most significant being in the transition-metal coordination in the trigonal prismatic site. The manganese atoms on this position are disordered onto sites toward the triangular faces of the prisms as observed in the Cu compound. However, refinements in which the trigonal-prismatically coordinated Zn atoms were disordered away from the center of the prism toward either the square or triangular faces gave poor fit parameters and resulted in the Zn position becoming unstable. A satisfactory refinement could only be achieved with the Zn on the special position 0, 0, $^1/_2$ at the center of the prism. In contrast to $Ba_6Mn_4CuO_{15}$, both of the octahedral transition-metal sites show a degree of occupational disorder. With the constraint of stoichiometry, the cation distribution over these sites was refined in a stepwise manner; the distribution over a pair of sites was refined to convergence, and then a different pair was refined to convergence and the process repeated until constant values for the fractional occupancies were obtained. This gave a final cation distribution of 0.930(4)Mn/0.070(4)Zn on M2, of 0.824(4)Mn/0.176(4)Zn on M3 and of 0.508(9)Mn/0.492(9)Zn on M1. A total of 57 variables were used in the final stages of the refinement. The resulting fits are shown in Figure 4 and have the residuals $R_{wp} = 10.96$, $R_p = 8.61$, $R_I = 12.88$, DW-d = 1.318 for the X-ray data and $R_{wp} = 7.86$, $R_p = 6.00$, $R_I = 6.53$, DW-d = 0.420 for the neutron data with a total $\chi^2_{red} = 3.553$. The atomic parameters are shown in Table 3, and the most important bond distances are shown in Table 4. A section of the polyhedral chain is shown in Figure 3b.

The data sets collected at 1.7 K for both compounds included three additional peaks of very low intensity that are not allowed nuclear reflections and that were absent from the room temperature data. This suggests that this intensity is due to long-range magnetic order, an unexpected observation in these highly

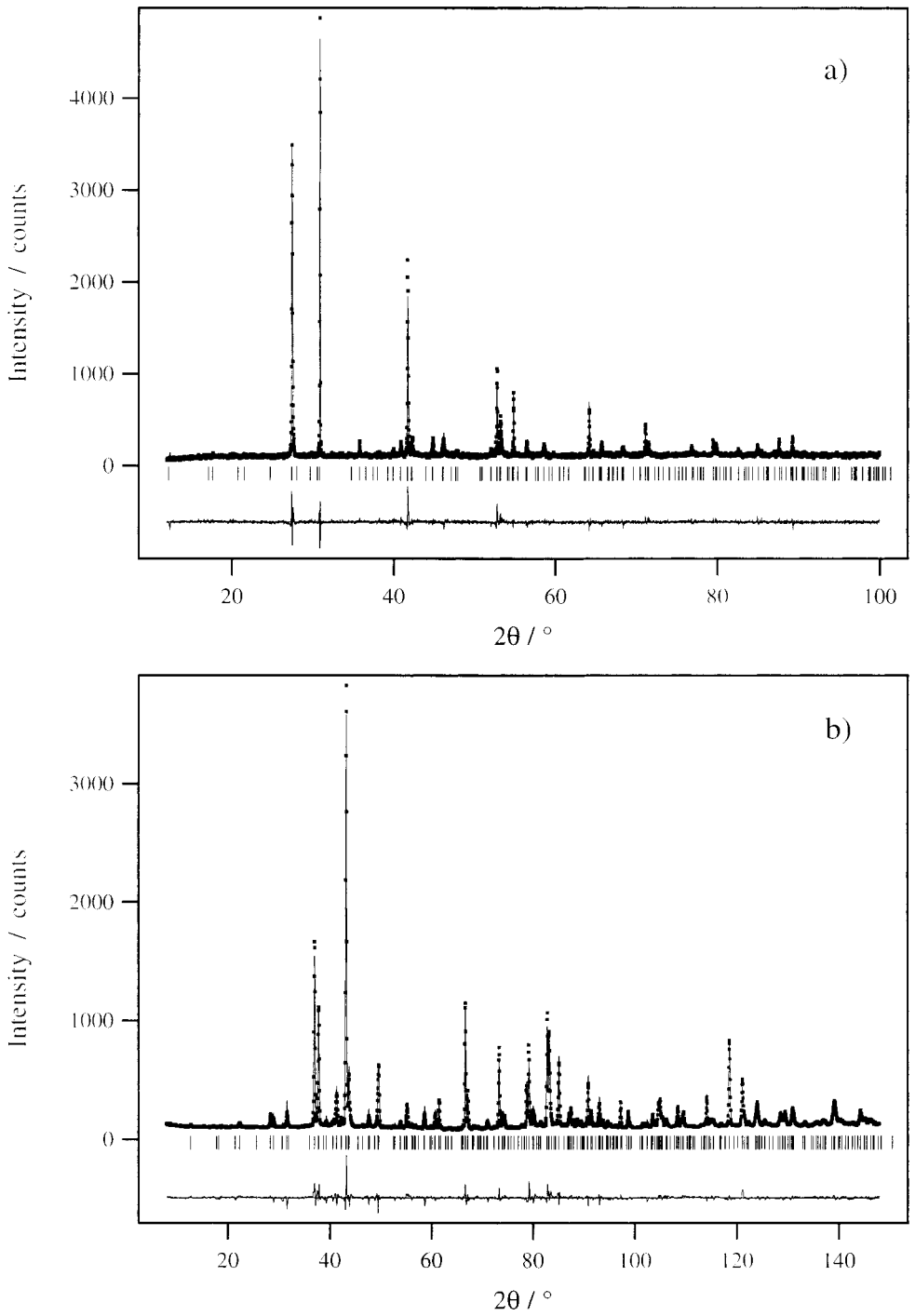

Figure 4. Observed (dots), calculated (full line), and difference X-ray (a) and neutron (b) diffraction patterns from $Ba_6Mn_4ZnO_{15}$ at room temperature. Reflection positions are indicated by tick marks.

anisotropic materials. The magnetic reflections could be indexed as 103, 203, and 213 reflections from a unit cell of the same size as the crystallographic unit cell. Several magnetic models were investigated in an attempt to fit the observed magnetic peaks in $Ba_6Mn_4CuO_{15}$. Trial models that only allowed a moment on the octahedral sites were considered, with both ferro- and antiferromagnetic coupling across the nonmagnetic trigonal prisms, and in models allowing a magnetic moment on the trigonal prismatic site (requiring a doubling of the *c*-axis) the sign of the interaction between the octahedra and the trigonal prisms was varied. No model based on a collinear spin arrangement could account for the observed intensity distribution. The only magnetic structure that did generate the observed diffraction pattern was the noncollinear model shown in Figure 5. In this model, the ordered moments on the octahedral sites are arranged in an antiparallel fashion in each chain, and no moment is observed on the trigonal prismatic site. The magnetic moments in the 0, 0, *z* chain are aligned along the *z*-direction, but the moments in the chains at $^1/_3,^2/_3, z$ and $^2/_3,^1/_3, z$ are rotated by 120° and 240°, respectively, in the *xz* plane. This results in the trigonal prismatic site being linked, by shared faces, to two octahedral sites which are antiparallel to each other.

This model was used to fit the 1.7 K neutron diffraction data in a manner similar to that described above for the room-temperature data set. The transition-metal ordering was constrained to be the same as that determined from the room-temperature data. The magnitude of the magnetic moment was refined, but the angle between moments in adjacent chains was

Table 3. Structural Parameters for $Ba_6Mn_4ZnO_{15}$ at Room Temperature[a]

	site	*x*	*y*	*z*	U_{iso}	frac
Ba(1)	9d	0.3269(4)	0	0	0.018(1)	
Ba(2)	9e	0.6547(4)	0	$^1/_2$	0.008(1)	
Zn(1)	3b	0	0	$^1/_2$	−0.0012(8)	0. 508(9)
Mn(1)[b]	6c	0	0	0.515(2)	−0.0012(8)	0.246(4)
M(2)	6c	0	0	0.0946(9)	−0.0012(8)	0.930(4)Mn/0.07(4)Zn
M(3)	6c	0	0	0.2835(9)	−0.0012(8)	0.824(4)Mn/0.176(4)Zn
O(1)	9d	0.8507(4)	0	0	0.008(9)	
O(2)	18f	0.4813(5)	−0.3335(6)	0.4790(3)	0.0182(9)	
O(3)	18f	0.8509(3)	0.0017(5)	0.6288(2)	0.0145(5)	

[a] Space group *R*32: $a = 10.0498(4)$ Å, $c = 12.8304(5)$ Å, $V = 1122.3(1)$ Å^3. [b] Disordered from center of trigonal prism. Trigonal prism has fractional occupancy 0.508(9)Zn/0.492(4)Mn.

Table 4. Bond Distances (Å) and Angles (deg) in $Ba_6Mn_4ZnO_{15}$ at Room Temperature

Ba(1)−O(1)	2.849(4) × 2	Zn(1)−O(3)	2.237(3) × 6
Ba(1)−O(2)	2.662(4) × 2	Mn(1)−O(3)	2.10(2) × 3
Ba(1)−O(2)	3.005(5) × 2	Mn(1)−O(3)	2.39(2) × 3
Ba(1)−O(3)	2.965(4) × 2	M(2)−O(1)	1.930(8) × 3
Ba(1)−O(3)	2.984(6) × 2	M(2)−O(2)	1.908(9) × 3
Ba(2)−O(1)	2.790(3) × 2	M(3)−O(2)	1.931(8) × 3
Ba(2)−O(2)	2.916(5) × 2	M(3)−O(3)	1.881(7) × 3
Ba(2)−O(2)	2.819(6) × 2	Zn(1)−M(3)	2.78(1)
Ba(2)−O(3)	2.566(4) × 2	Mn(1)−M(3)	2.58(3)
Ba(2)−O(3)	3.174(3) × 2	M(3)−M(2)	2.42(2)
shortest O(2)−O(2)	2.577(7)	M(2)−M(2)	2.43(2)
O(3)−Zn(1)−O(3)	71.4(1)	Zn(1)−O(3)−M(3)	84.4(3)
O(3)−Zn(1)−O(3)	95.3(1)	M(3)−O(3)−Mn(1)	80.7(7)
O(1)−M(2)−O(2)	95.2(1)	M(3)−O(3)−Mn(1)	87.5(4)
O(2)−M(3)−O(3)	93.9(2)	M(2)−O(1)−M(2)	77.9(5)
O(3)−Mn(1)−O(3)	94.8(2)		

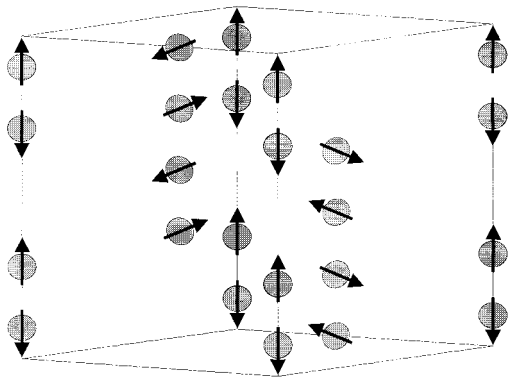

Figure 5. Magnetic structure observed in $Ba_6Mn_4MO_{15}$. Only transition metals occupying octahedrally coordinated sites are shown.

fixed at the ideal value of 120° due to the extremely low intensity of the magnetic reflections. The angular dependence of the magnetic scattering amplitude was described by the free-ion form factor[13] for Mn^{4+}, and the magnitude of the magnetic moment was constrained to be the same on each octahedral site; our data were not good enough to enable us to allow for the different cation occupancies of the different sites. Preliminary refinements indicated there was no ordered moment on the prismatic site in either compound. The final value for the refined moment from the $Ba_6Mn_4CuO_{15}$ data was 0.16(2) μ_B per octahedral site, giving the fit shown in Figure 6 and the residuals $R_{wp} = 7.01$, $R_p = 5.25$, $R_I = 6.06$, DW-d = 0.499, and $\chi^2_{red} = 4.532$ for 45 variables. The final atomic parameters are shown in Table 5. The data collected from $Ba_6Mn_4ZnO_{15}$ were fitted in a similar way and the model refined to give an ordered magnetic moment of 0.12(3) μ_B per octahedral site and the residuals $R_{wp} = 8.66$, $R_p = 6.65$, $R_I = 6.15$, DW-d = 0.378 and $\chi^2_{red} = 7.397$ for 40 variables. The final atomic coordinates are shown in Table 6. The magnetic susceptibility data collected from $Ba_6Mn_4ZnO_{15}$ did not show a field dependence, and only the data collected in a field of 100 G are shown in Figure 7. The field-cooled and zero-field-cooled data overlie in the temperature range measured and show a broad local maximum at 40(5) K. A Curie−Weiss law could not be used to describe the temperature dependence of the susceptibility over any of the measured temperature range. The susceptibility passes through a local minimum and increases below 16(1) K, but the observed increase could not be fitted by a Curie−Weiss law. Unfortunately, our magnetometer was unable to maintain stable temperatures below 4.2 K for long enough to measure *M*(H) at 1.7 K; the temperature at which the neutron diffraction experiments showed magnetic order to be present. However, *M*(H) was measured at 5 K and was linear as shown in Figure 8.

The magnetic susceptibility of $Ba_6Mn_4CuO_{15}$ differs considerably from that of $Ba_6Mn_4ZnO_{15}$, and the data collected in a field of 100 G are shown in Figure 9. The susceptibility did not show a field dependence. There is a sharp maximum at 5(1) K below which the field-cooled and zero-field-cooled data diverge. Figure 9 also shows the calculated spin-only contribution to the susceptibility from 0.669 mol of paramagnetic $S = {}^1/_2$, d,[9] Cu^{2+}, that is the amount of Cu occupying the trigonal

Table 5. Structural Parameters for $Ba_6Mn_4CuO_{15}$ at 1.7 K[a]

	site	*x*	*y*	*z*	U_{iso}
Ba(1)	9d	0.3277(6)	0	0	0.009(2)
Ba(2)	9e	0.6556(6)	0	$^1/_2$	0.004(2)
Cu(1)	9d	0.940(1)	0.940(1)	$^1/_2$	−0.0009(8)
Mn(1)	6c	0	0	0.530(4)	−0.0009(8)
M(2)	6c	0	0	0.0958(9)	−0.0009(8)
M(3)	6c	0	0	0.286(2)	−0.0009(8)
O(1)	9d	0.8492(6)	0	0	−0.003(1)
O(2)	18f	0.4820(6)	−0.3330(8)	0.4801(3)	0.012(1)
O(3)	18f	0.8503(6)	0.0018(6)	0.6300(3)	0.0157(7)

[a] Space group *R*32: $a = 10.0211(3)$ Å, $c = 12.8241(4)$ Å, $V = 1115.28(9)$ Å^3.

Table 6. Structural Parameters for $Ba_6Mn_4ZnO_{15}$ at 1.7 K[a]

	site	*x*	*y*	*z*	U_{iso}
Ba(1)	9d	0.3273(7)	0	0	0.014(2)
Ba(2)	9e	0.6554(5)	0	$^1/_2$	0.003(1)
Zn(1)	9d	0.940(1)	0.940(1)	$^1/_2$	−0.005(1)
Mn(1)	6c	0	0	0.515(2)	−0.005(1)
M(2)	6c	0	0	0.096(1)	−0.005(1)
M(3)	6c	0	0	0.278(1)	−0.005(1)
O(1)	9d	0.8505(5)	0	0	−0.003(1)
O(2)	18f	0.4818(7)	−0.3335(8)	0.4787(3)	0.014(1)
O(3)	18f	0.8504(5)	0.0022(6)	0.6285(2)	0.0078(7)

[a] Space group *R*32: $a = 10.0233(6)$ Å, $c = 12.7988(8)$ Å, $V = 1113.6(2)$ Å^3.

(13) Crystallography, I. U. of *International Tables for Crystallography* 4th ed.; Kluwer Academic Publishers: Dordrecht, 1995; Vol. C.

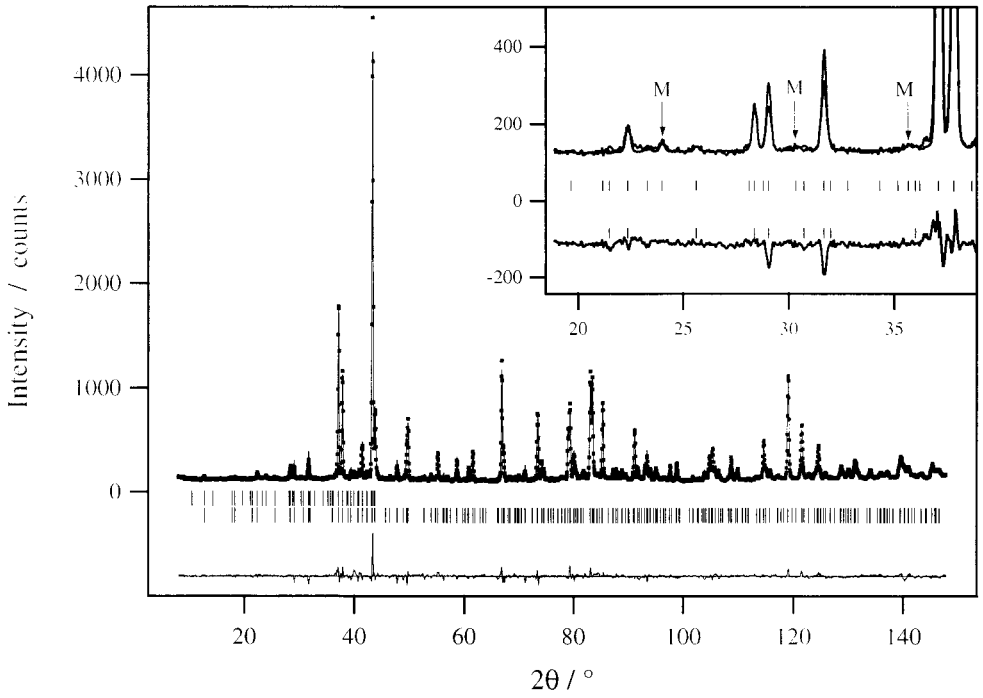

Figure 6. Observed (dots), calculated (full line), and difference neutron diffraction patterns from $Ba_6Mn_4CuO_{15}$ at 1.7 K. Nuclear reflections are indicated by the upper set of tick marks and allowed nuclear reflections by the lower set. The inset show the region of the pattern containing the magnetic reflections.

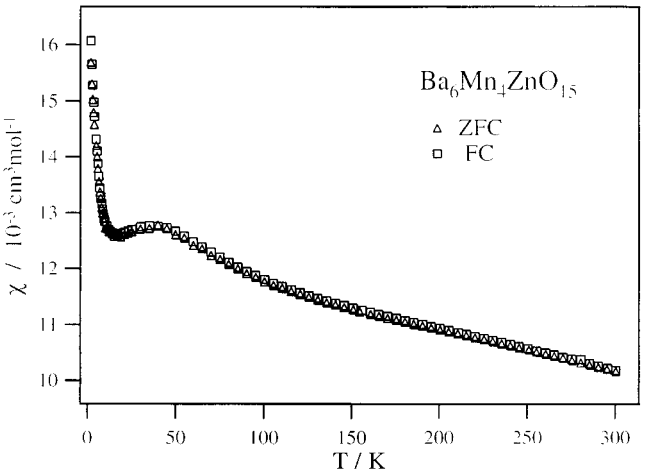

Figure 7. Molar magnetic susceptibility of $Ba_6Mn_4ZnO_{15}$ recorded in 100 G after cooling in zero field (triangles) and the measuring field (squares) as a function of temperature.

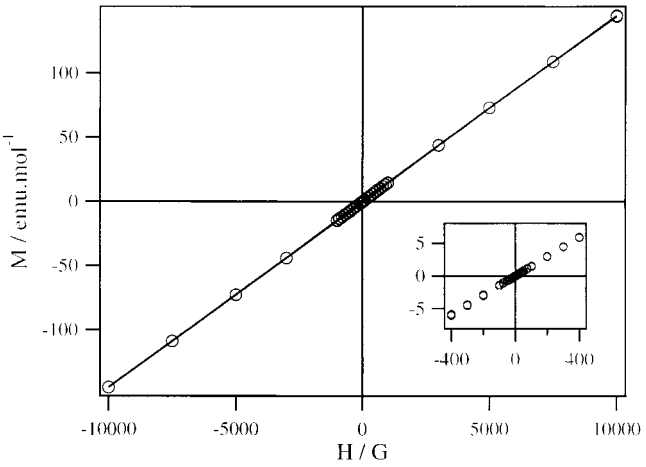

Figure 8. Plot of magnetization of $Ba_6Mn_4ZnO_{15}$ against applied field measured at 5 K after cooling the sample from room temperature in a field of 10 kG. The inset shows data around the origin.

prismatic site. The increase in the susceptibility in the temperature range $5 < T/K < 300$ can clearly be accounted for by these cations alone. The residual susceptibility (inset) is similar in both magnitude and temperature dependence to that observed (Figure 7) in $Ba_6Mn_4ZnO_{15}$, although the broad maximum has moved to ca. 90 K. The magnetization (Figure 10) at 5 K shows a slight nonlinear variation with field; the measurement was repeated at 25 K, and the magnetization showed a linear field dependence.

Discussion

The availability of neutron diffraction data has allowed the refinement of more parameters than would have been possible from X-ray data alone. In the case of $Ba_6Mn_4CuO_{15}$, the displacement of Cu from the center of the trigonal prismatic sites toward the square faces was clearly indicated in the difference Fourier map calculated from the neutron data but was not detected by the X-ray diffraction experiment. Cu^{2+} has the electronic configuration d^9 and the displacement of the cation to adopt (pseudo-) square-planar geometry will remove the degeneracy of the electronic ground state and hence lower the electronic energy. A comparable displacement has been observed in closely related compounds Sr_3CuIrO_6[14] and Sr_3CuPtO_6,[15] both $n = \infty$ members of the series, in which the octahedral sites are occupied exclusively by Pt and the trigonal prismatic sites by Cu. In these compounds, the Cu is fully ordered into the square-planar faces and so results in a reduction in symmetry to the monoclinic space group *C*2/*c*. Conversely, the compound $Ba_6Ir_4CuO_{15}$ shows considerable disorder between the transition metals; the trigonal prismatic site contains only 36(2)% Cu,

(14) Neubacher, M.; Muller-Buschbaum, H. *Z. Anorg. Allg. Chem.* **1992**, *607*, 124.

(15) Wilkinson, A. P.; Cheetham, A. K.; Kunnman, W.; Kvick, A. *Eur. J. Solid State Inorg. Chem.* **1991**, *28*, 453.

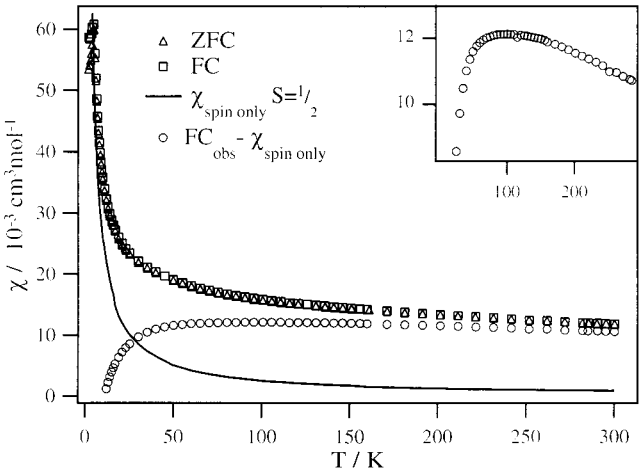

Figure 9. Molar magnetic susceptibility of $Ba_6Mn_4CuO_{15}$ recorded in 100 G as a function of temperature. The plot shows the susceptibility after cooling in zero field (triangles) and the measuring field (squares) as well as the calculated spin only contribution from 0.669 mol Cu^{2+} and the observed field cooled susceptibility after subtraction of the paramagnetic Cu^{2+} contribution (also shown in inset).

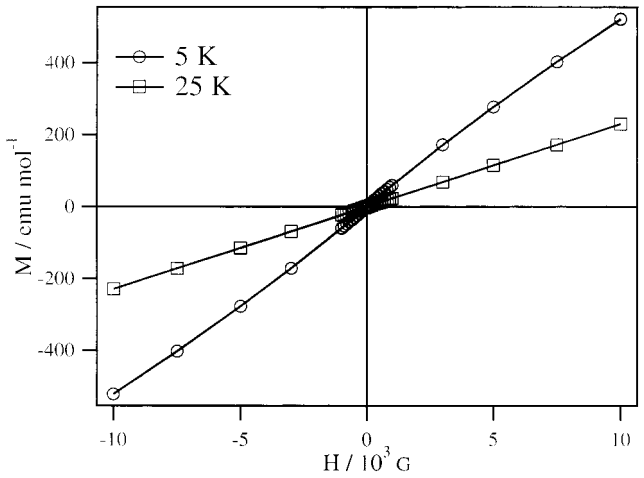

Figure 10. Plot of magnetization of $Ba_6Mn_4CuO_{15}$ against applied field measured at 5 K (circles) and 25 K (squares) after cooling the sample from room temperature in a field of 10 kG.

which is found at the center of the prism.[16] It is believed that the Cu displacement is quenched by the presence of a substantial amount of Ir on this site. In $Ba_6Mn_4CuO_{15}$, the neutron diffraction data show that the trigonal prismatic site has a Cu occupation, 67(1)%, intermediate between these two values, and that the Cu is displaced from the center in a disordered manner so as to achieve pseudo-square-planar coordination, but with no reduction to monoclinic symmetry. We believe that the partial occupation of the trigonal prisms by Mn prevents the long-range ordering of the Cu displacement which lowers the symmetry.

The displacement of the Mn from the center of the trigonal prisms toward the triangular faces, which is observed in both of the phases reported here, can be rationalized if the size of the trigonal prismatic interstice is considered. If Mn were constrained on the ideal 0, 0, $^1/_2$ position the Mn−O distance would have been ca. 2.2 Å compared to the values typically found in other Mn^{4+} compounds (ca. 1.9 Å). The transition metal−oxygen bond distances in the face sharing octahedral sites are close to this value.

(16) Battle, P. D.; Blake, G. R.; Darriet, J.; Weill, F. *J. Mater. Chem.* **1997**, *7*, 1559.

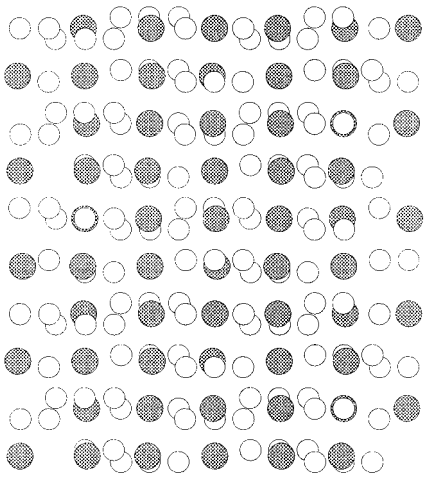

Figure 11. Layers of Ba_3O_9 from $Ba_6Mn_4ZnO_{15}$ viewed along [110]. Dark circles represent Ba cations and light circles represent oxide ions.

The Zn−O distance in the trigonal prismatic site of $Ba_6Mn_4ZnO_{15}$ is considerably longer than that observed in the octahedral sites, more so than in the isostructural compounds $Ba_6Ni_5O_{15}$[7] and $Sr_6Co_5O_{15}$.[8] This is in keeping with the ionic radius of Zn^{2+} being larger than Mn^{4+} in 6-fold coordination[17] and so is not unexpected. However, it is interesting to note the flexibility of the oxygen polyhedral chain in accommodating this variation in cation sizes. The results of our structure determination also demonstrate that although these materials are schematically described in terms of hexagonally stacked layers, the usefulness of this approach is limited as considerable distortion can result in buckling of the layers, Figure 11. No significant changes were apparent in either the metal−oxygen distances or the metal−metal distances on cooling from room temperature to 1.7 K.

The magnetic properties of these two compounds are very complex. Compounds belonging to this structural family have been widely studied in the belief that they will show unusual 1-dimensional electronic behavior. However, our observation of magnetic peaks in the neutron diffraction pattern indicates that superexchange between the transition-metal chains cannot be ignored. The molar magnetic susceptibility of $Ba_6Mn_4ZnO_{15}$ is low compared to the Curie law value and only weakly temperature dependent throughout the measured temperature range. This leads us to assume that the short-range antiferromagnetic interactions between Mn^{4+} cations in face-sharing octahedra are significant at 300 K. In a structurally ordered chain, these interactions might, on cooling, lead first to 1-dimensional antiferromagnetism, but the chains in $Ba_6Mn_4ZnO_{15}$ are nonideal in that they periodically contain an enlarged polyhedron (a prism) and that there is a partially disordered arrangement of magnetic Mn^{4+} and diamagnetic Zn^{2+} over the polyhedral sites. It is likely that the broad maximum observed in the magnetic susceptibility at 45(5) K represents the onset of 1-dimensional ordering along individual chains and that the rise in the susceptibility at lower temperatures stems from Mn^{4+} cations, on either octahedral or prismatic sites, that possess uncompensated magnetic moments as a consequence of structural disorder. The temperature at which the transition to long-range 3-dimensional magnetic order occurs is not apparent in the susceptibility data. This is because it is a transition from 1-dimensional antiferromagnetism to 3-dimensional antiferromagnetism and there is, therefore, no reduction in the observed moment.

(17) Shannon, R. D.; Prewitt, C. T. *Acta Crystallogr.* **1969**, *B25*, 925.

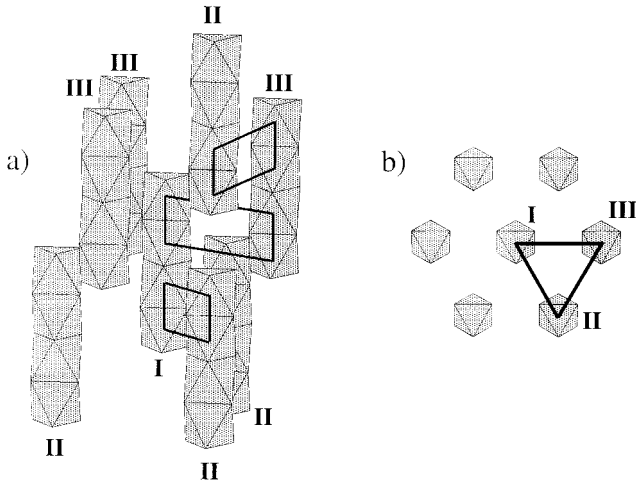

Figure 12. Magnetic interactions (a) occurring in $Ba_6Mn_4MO_{15}$ and (b) shown in projection along [001]. The central tetramer (**I**) has six nearest neighbors. The three tetramers **II** interact with the lower two octahedra of **I** and the three tetramers **III** interact with the upper two octahedra of **I**. The **I**−**II** and **I**−**III** interactions are equivalent.

The behavior of $Ba_6Mn_4CuO_{15}$ is somewhat different from that of the Zn analogue. The data plotted in Figure 9 suggest that 1-dimensional ordering occurs at 90(5) K and that the relatively large increase in the susceptibility observed at lower temperatures can be accounted for if just the Cu^{2+} cations in the prismatic sites remain paramagnetic. This interpretation implies that all the other Mn^{4+} and Cu^{2+} cations, including prismatically coordinated Mn^{4+}, are antiferromagnetically coupled. The paramagnetism of the prismatic Cu^{2+} cations might stem from their displacement off the axis of the prism, but it is also possible that the agreement (Figure 9) between the observed paramagnetism and that expected from the prismatic Cu^{2+} is fortuitous and that other cations are involved. However, the occurrence of a spin freezing transition at 5 K in $Ba_6Mn_4CuO_{15}$, but not in $Ba_6Mn_4ZnO_{15}$, does support the idea that the Cu^{2+} cations are central to this behavior. We believe, although we have no proof, that spin-freezing among the decoupled spins is likely to coincide with the onset of long-range antiferromagnetism among the 1-dimensional spin-ordered units. Further neutron diffraction experiments are needed to resolve this point.

The magnetic structure adopted by these compounds is unusual and certainly more complex than those of the $n = \infty$ phases $Ca_3Co_2O_6$[18] and Ca_3MRuO_6 (M = Na, Li),[19] the only other mixed-layer compounds for which a magnetic structure has been reported. The best starting point for a discussion of the magnetic structure is a consideration of idealized $Ba_6Mn_4ZnO_{15}$, in which all the octahedra are occupied by Mn^{4+}, and the prisms by Zn^{2+}. We assume that the interaction between neighboring, face-sharing sites in each [001] chain of transition metals is antiferromagnetic, as are those across a diamagnetic prismatic site and between nearest-neighbor cations in adjacent chains; the latter two assumptions are consistent with the magnetic structures[19] of $n = \infty$ Ca_3MRuO_6 (M = Na, Li), which contain a d^3 cation (Ru^{5+}) similar to Mn^{4+}. With reference to Figure 12, two neighboring cations in a particular tetramer in chain **I** are thus expected to interact antiferromagnetically with two neighboring sites in chain **II**. The other two neighboring cations in the chain **I** tetramer will interact antiferromagnetically with two neighboring sites in chain **III**. However, the adoption of this scheme to satisfy the requirements of chain **I** results in ferromagnetic alignment between nearest neighbor cations in chains **II** and **III**. The adoption of a collinear magnetic structure is thus frustrated, with the consequence that a noncollinear, 120°, spin structure is adopted. There is thus a certain similarity between the idealized $n = 1$ phase, built up from a mixture of A_3O_9 and $A_3A'O_6$ layers, and the Kagome lattice of the 2H perovskites,[20] built up from A_3O_9 layers only. The principal difference between $Ba_6Mn_4MO_{15}$ and the 2H structures is that an octahedral site in the former has only three neighboring sites in adjacent chains, whereas in the latter there are six. It is difficult to assess the effect of cation disorder on this model. Half of the prismatic sites in $Ba_6Mn_4ZnO_{15}$ are occupied by Mn^{4+} cations that are displaced toward one of the adjacent tetramers. Consequently, approximately 12% of the octahedral sites are occupied by Zn^{2+}, thus creating magnetic trimers, dimers, and isolated octahedra. The susceptibility shows a low concentration of free moments at 2 K and no hysteresis characteristic of random spin freezing, yet the 3-dimensional ordered component of the magnetic moment measured by neutron diffraction is very low on the octahedral sites and undetectably small in the prisms. Although the ordered moment in frustrated 2H $CsVCl_3$, again containing a d^3 cation, is reduced to 40% of the expected value[21] by zero-point motion, the reduction is much greater in $Ba_6Mn_4ZnO_{15}$. These observations suggest that the majority of the spins in the latter compound are involved in short-range or 1-dimensional ordering but that the introduction of disorder into the superexchange pathways causes a very large reduction in the 3-dimensional ordered moment. The most significant perturbation to the idealized magnetic model might be expected to be caused by the presence of a magnetic cation on 50% of the prismatic sites, assumed to be nonmagnetic in the ideal structure. However, both the Mn−O and the Mn−Mn distances around this site are significantly longer that those around the octahedral sites, and the magnetic effects will be correspondingly weaker. The ordered spin structure observed in $Ba_6Mn_4CuO_{15}$ is essentially the same as that of the Zn analogue, despite the fact that the Mn concentration in the prisms is lowered and that all the prisms are now occupied by a magnetic cation. This strengthens the hypothesis that the prismatic Mn cations do not play a key role in determining the magnetic structure. The absence of an ordered magnetic moment on the prismatic Cu site is consistent with the suggestion, made above on the basis of the susceptibility data, that the spins of the four-coordinate cations freeze at 5 K, giving rise to the hysteresis effects which are not seen when the relevant cation is diamagnetic Zn^{2+}. The nonlinearity of M(H) at 5 K seen for $Ba_6Mn_4CuO_{15}$, but not for $Ba_6Mn_4ZnO_{15}$, may be symptomatic of this spin freezing.

It is interesting to note that the related 2H perovskite $BaMnO_3$ has been the subject of a low-temperature (1.8 K) neutron diffraction study[22] that detected three magnetic peaks that were indexed as 101, 201, 211 reflections by utilizing a magnetic unit cell with the same c parameter as the crystallographic unit cell (4.806 Å) and $a_{mag} = \sqrt{3}a_{cryst}$, i.e., containing three transition metal chains within the unit cell, as is the case for $Ba_6Mn_4MO_{15}$. Christensen et al. fitted their neutron diffraction data using a magnetic model in which the ordered moment, ca. 3 μ_B, was orientated in the *z* direction and arranged antiferro-

(18) Aasland, S.; Fjellvag, H.; Hauback, B. *Solid State Commun.* **1997**, *101*, 187.

(19) Battle, P. D.; Blake, G. R.; Burley, J. C.; Cussen, E. J.; Sloan, J.; Vente, J. F.; Darriet, J.; Weill, F. *Mater. Res. Soc. Symp. Proc.* **1998**, *547*, in press.

(20) Zandbergen, H. W. *J. Solid State Chem.* **1980**, *35*, 367.

(21) Hirakawa, K.; Yoshizawa, H.; Ubukoshi, K. *J. Phys. Soc. Jpn.* **1982**, *51*, 1119.

(22) Norland-Christensen, A.; Ollivier, G. *J. Solid State Chem.* **1972**, *4*, 131.

magnetically along each chain. The magnetic moments of the metals at $^1/_3$, $^2/_3$, 0 and $^2/_3$, $^1/_3$, 0 were arranged antiparallel to the moment at 0, 0, 0. Their proposed structure can therefore be described in terms of ferrimagnetic layers stacked antiferromagnetically in the *z*-direction. On the basis of simulated diffraction patterns, we believe that the magnetic peaks observed in $BaMnO_3$ could be fitted using a canted spin arrangement similar to that described above for $Ba_6Mn_4MO_{15}$, thus eliminating the need for ferromagnetic coupling between an arbitrarily chosen pair of chains. Christensen et al. also measured the magnetic susceptibility in the temperature range $2.3 < T/K < 300$ and failed to detect a maximum, which they ascribed to the difference in the minimum measured temperatures in the different experiments. However, given our similar observation in $Ba_6Mn_4ZnO_{15}$, we suggest that variable-temperature neutron diffraction is the only way to unambiguously determine the temperature at which long-range magnetic ordering occurs in these strongly anisotropic materials. We plan to carry out further low-temperature neutron diffraction experiments in order to establish any correlation between the magnetic moment on a given octahedral site and the manganese occupancy. We also hope to establish the reason for the very low ordered moment in $Ba_6Mn_4CuO_{15}$ and $Ba_6Mn_4ZnO_{15}$; we expect to find a dependence on the degree of chemical disorder.

Acknowledgment. We are grateful to EPSRC for financial support and to T. Hansen for experimental assistance at ILL, Grenoble.

JA984313U